Vibrationally resolved transition state spectroscopy of the F + H_2 and F + CH_4 reactions†

Tara I. Yacovitch,[a] Etienne Garand,‡[a] Jongjin B. Kim,[a] Christian Hock,[a] Thomas Theis[a] and Daniel M. Neumark*[ab]

Received 28th January 2012, Accepted 15th February 2012
DOI: 10.1039/c2fd20011b

The transition state regions of the F + *para*-H_2, F + *normal*-H_2, F + CH_4 and F + CD_4 reactions have been studied by slow electron velocity-map imaging (SEVI) spectroscopy of the anionic precursor clusters *para*-FH_2^-, *normal*-FH_2^-, FCH_4^- and FCD_4^-. The F + H_2 results improve on previously published photoelectron spectra, resolving a narrow peak that appears in the same position in the *para*-FH_2^- and *normal*-FH_2^- spectra, and suggesting that additional theoretical treatment is necessary to fully describe and assign the experimental results. A small peak in the *para*-FH_2^- results is also identified, matching simulations of a product resonance in the $v' = 3$ vibrational level. SEVI spectra of the $^2P_{3/2}$ bands of FCH_4^- and FCD_4^- show extended structure from transitions to the entrance valley van der Waals region and the reactant side of the F + CH_4 transition state region. Much of this structure is attributed to bending or hindered rotation of the methane moiety and may be a spectroscopic signature of reactive resonances.

I. Introduction

The F + H_2 → FH + H reaction and its various isotopologs have been extensively studied as the quintessential bimolecular reaction.[1–4] The F + CH_4 → FH + CH_3 reaction has evolved into a benchmark polyatomic reaction and provides insight into how additional degrees of vibrational freedom affect chemical reaction dynamics.[5–7] Exploration of the potential energy surfaces for these reactions can be accomplished by crossed molecular beam experiments[8,9] where the characteristics of the surface are gleaned from the cross sections, angular distribution and states of the final products. Negative ion photoelectron (PE) spectroscopy[10] can complement these studies by directly accessing the transition state region *via* photodetachment of an anion with appropriate geometry. In the case of the F + H_2 and F + CH_4 reactions, the corresponding FH_2^- and $F^-(CH_4)$ anions have good geometric overlap with the neutral transition state region[11,12] and hence directly probe the spectroscopy of this critically important region of the reactive surface. In this work, we employ slow electron velocity-map imaging (SEVI), a high resolution variant of anion PE spectroscopy, to obtain significantly improved results for both systems.

[a]*Department of Chemistry, University of California, Berkeley, CA 94720, USA. E-mail: dneumark@berkeley.edu; Fax: +1 510 642 3635; Tel: +1 510 643 3850*
[b]*Chemical Sciences Division, Lawrence Berkeley National Laboratory, faraBerkeley, CA 94720, USA*

† Electronic supplementary information (ESI) available: sample data workup for FH_2^- showing parallel and perpendicular spectra. Original data sets for FCH_4^- and FCD_4^- showing invariance of peak positions. See DOI: 10.1039/c2fd20011b

‡ Current address: Sterling Chemistry Lab, Yale University, New Haven, CT 06520, USA

Negative ion photoelectron (PE) spectra of the FH_2^- anion, have been reported previously.[11, 13–15] These spectra show resolved hindered rotor progressions associated with the F + H_2 transition state region. The structure of these progressions depends on whether the F^- is complexed to *para* or *normal* H_2. Given that the anion is linear, the observation of a hindered rotor progression suggests that the neutral transition state (TS) is bent. This interpretation is supported by extensive theoretical work on the $FH_2 \leftarrow FH_2^-$ system,[11,16,17] which reproduced the main experimental features *via* exact quantum scattering calculations on the best potential energy surfaces available at the time. In the original PE spectra, the peak widths were about 19 meV wide, with a good fraction of this arising from the experimental resolution of around 12 meV, raising the question of what additional structure might be seen at higher experimental resolution.

To address this point, Russell and Manolopoulos (RM) performed time-dependent wavepacket simulations of FH_2^- photoelectron spectra[16] on the *ab initio* potential energy surface calculated by Stark and Werner (SW-PES).[18] These simulations predict sharp resonance peaks and broader direct scattering peaks that are clearly separable at a resolution of 1 meV, but not at the lower resolution of the experimental PE spectra. Hartke and Werner[17] (HW) subsequently made adjustments to the potential energy surface (HSW-PES) to include spin–orbit coupling, and new photoelectron spectroscopy simulations using a more realistic anharmonic potential for the anions were performed. Since then, a number of highly sophisticated surfaces have been published.[19–23] These post-SW surfaces have proven accurate in the description of various crossed-molecular beam results, but have not yet been used to simulate the $FH_2 \leftarrow FH_2^-$ negative ion photoelectron spectra.

Liu and co-workers[7] have performed extensive experimental work on the F + CH_4 reaction and its isotopologs, and several potential energy surfaces for this reaction have been published recently.[24–28] Recent negative ion photoelectron spectra of FCH_4^- have been published by Cheng *et al.*[12] These spectra show two broad bands which were assigned to the atomic fluorine $^3P_{3/2}$ and $^3P_{1/2}$ spin orbit (SO) states, shifted to a larger splitting by the proximity of the methane. The experimental spin orbit (SO) splitting was compared to SO splittings taken from calculated energies for the ground and excited state neutral surfaces, revealing that the photodetachment accesses a region on the ground state F + CH_4 potential between the reactant van der Waals (vdW) well and the TS. Simulated photoelectron spectra for this system have not been calculated, though Bowman and coworkers have recently published an *ab initio* surface for both the FCH_4^- anion[29] and the F + $CH_4 \rightarrow$ FH + CH_3 neutral surface.[28,30] Their anion calculations support previous findings[31] of a $F^-\cdots H–CH_3$ C_{3v} equilibrium geometry. Their neutral calculations reveal an early TS with a bent $F\cdots H–CH_3$ geometry, as well as two reactant vdW structures with C_{3v} geometries, with the deeper minimum corresponding to a $F\cdots H_3CH$ structure.

In this paper, we investigate the F + H_2 and F + CH_4 systems *via* SEVI of FH_2^- and FCH_4^- to see what additional structure can be observed at higher resolution than in previously reported work. Fig. 1 shows potential energy diagrams of both systems along the hydrogen transfer reaction coordinate, illustrating the geometric overlap between the anion and neutral surface. In both cases, the anion has good overlap with the neutral TS region and, possibly, bound vdW states in the reactant valley. We thus expect to observe vibrational progressions in one or more modes perpendicular to the reaction coordinate in the TS region,[32] sharp structure from the vdW states,[33] and, possibly, reactive resonances. The latter are from quasibound quantum states, localized along the reaction coordinate, such as those seen in the I + HI $\rightarrow$ IH + I reaction *via* zero electron kinetic energy (ZEKE) spectroscopy on IHI^-.[34]

The observation and identification of reactive resonances is a key goal in transition state spectroscopy as these relatively long-lived states are very sensitive to the transition state region of the potential energy surface.[32,35] There is considerable

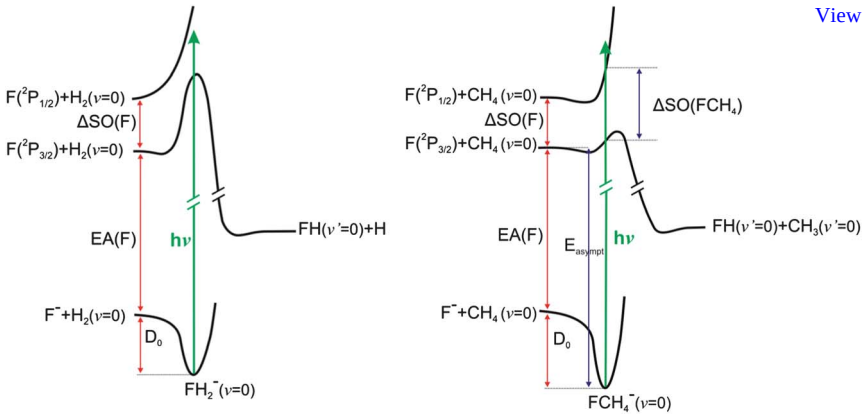

Fig. 1 Potential energy diagram (not to scale) for the F + H_2 and F + CH_4 systems. Vibrationally adiabatic curves (potential energy + zero point energy) are shown for the anion and neutral along with a green arrow (hν) indicating the approximate regions accessed by photodetachment. Relevant energies are labeled: the anion well depth, D_0; fluorine atom electron affinity, EA(F) and spin orbit splitting, ΔSO(F); neutral FCH_4 spin orbit splitting at the anion geometry, ΔSO(FCH_4). The electron binding energy to the ground state reactant asymptote is labeled E_{asympt} and is used as an energetic reference.

evidence from scattering experiments and calculations supporting the presence of resonances for the two reactions considered here. It was only in 2000 that Skodje *et al.* definitively identified a reactive resonance in the integral cross section of the F + HD reaction.[36] This resonance corresponds to a state with three vibrational quanta in the HF product and all other quantum numbers zero: HF($v' = 3$) + D. Subsequent studies on differential cross sections and product state distributions validate this assignment and further characterize this resonance.[23,37-39] Around this same time, Shiu *et al.* reported the first experimental signs of a reactive resonance in the F + $CH_4 \rightarrow$ FH + CH_3 reaction with similar origins as the one in the F + HD results: FH($v' = 3$) + CH_3.[5] Evidence for this same resonance then emerged for the F + CHD_3 and F + CD_4 isotopomers.[40,41] The SEVI work presented here offers the opportunity to observe the direct spectroscopic signature of resonances associated with these reactions as sharp spectral features.

II. Experimental methods

SEVI is a high-resolution variant of negative-ion photoelectron spectroscopy and has been described in detail previously.[42,43] Briefly, negative ions are photodetached with a tunable laser, and the slow electrons are selectively detected using a low-voltage extraction velocity-map imaging (VMI) setup.[44] By varying the detachment wavelength, a number of high-resolution scans over limited energy windows are obtained.

Anions were produced by expanding an appropriate gas mixture, at a stagnation pressure of 250–400 psi, into the source vacuum chamber through an Even-Lavie pulsed valve.[45] FH_2^- anions were formed using a grid discharge source,[46] and FCH_4^-/FCD_4^- anions using a circular ionizer and water-cooled jacket for the valve.[47] *Normal*-FH_2^- (*n*-FH_2^-) anions were produced using a gas mix containing trace NF_3 and 10% to 24% H_2 in a balance of argon. A similar mix using parahydrogen (*p*-H_2) was used to make the *para*-FH_2^- ions (*p*-FH_2^-). *p*-H_2 was produced in the setup of Theis *et al.*[48] to a purity of 95%. In order to prevent back-conversion to *ortho*-H_2, all stainless steel except for the interior surface of the pulsed valve was removed from the gas manifold. FCH_4^- anions were produced with trace NF_3, 10% CH_4 and a balance of argon. FCD_4^- was similarly made with trace NF_3 in 3% CD_4/argon mix.

Ions were mass-selected[49] and directed to the detachment region by a series of electrostatic lenses and pinholes. They were then photodetached between the repeller and the extraction plates of the VMI assembly by the frequency-doubled output of a Nd:YAG-pumped tunable dye laser. The resulting photoelectron cloud was coaxially extracted down a 50 cm flight tube and mapped onto a detector comprising micro-channel plates coupled to a phosphor screen.[50,51] Events on the screen were collected by a 1024 × 1024 Charge-Coupled Device (CCD) camera and sent to a computer, where they were summed, centered, smoothed, quadrant-symmetrized and transformed using the inverse-Abel[52] or pBasex[53] methods. Centering of images is crucial for high resolution results after transformation[54] so a F^- or Cl^- image was used as a reference.

Photoelectron kinetic energy spectra were obtained by angular integration of the transformed images. SEVI spectra are plotted with respect to electron binding energy (eBE), defined as the difference between the photodetachment photon energy and the measured electron kinetic energy (eKE). In each SEVI image, better energy resolution was obtained for slower electrons. Hence, by varying the photodetachment laser wavelength, overview and detailed scans can be obtained.

SEVI also provides information on the photoelectron angular distribution (PAD).[51] The anisotropy of the photoelectron images is determined by the angular momenta of the photoelectron partial waves, which, in turn, reflect the shape of the orbital from which detachment occurs. *s*-wave ($\ell = 0$) detachment results in isotropic images, while *p*-wave ($\ell = 1$) detachment peaks at 0° and 180° relative to the laser polarization axis.

The apparatus was calibrated by acquiring SEVI images of atomic Cl^- at several different photon energies.[55,56] VMI repeller voltages of −350 and −200 V were used in this study. For an ideal system of atomic transitions, with *s*-wave character, intense ion signal, and well-spaced easy-to-center peaks, the SEVI instrument can easily surpass 1 meV resolution. For a Cl^- peak using −350 V VMI repeller voltage, fwhm of 3.7 cm^{-1} (0.46 meV) at 22 cm^{-1} from threshold and 9.4 cm^{-1} (1.2 meV) further out at 161 cm^{-1} from threshold are achieved. Using a −200 V VMI repeller voltage, a fwhm of 2.5 cm^{-1} (0.31 meV) is achieved 16.0 cm^{-1} from threshold. This is our instrumental resolution. However, linewidths in the FH_2^- spectra are limited because, as shown below, photodetachment occurs mainly by emission of *p*-wave electrons ($\ell = 1$). The photodetachment cross section σ drops off severely close to threshold for *p*-wave detachment according to the Wigner threshold law, $\sigma \propto (eKE)^{l+1/2}$.[57] One must therefore collect data at photon energies further from the threshold than for *s*-wave ($\ell = 0$) detachment, limiting the ultimate resolution of the SEVI spectra.

III. Results and analysis

Smoothed and symmetrized photoelectron images at 311 nm for *p*-FH_2^- and 332 nm for FCH_4^- are shown in Fig. 2. These images are dominated by *p*- and *s*-wave detachment, respectively, with the former leading to a PAD peaked along the laser polarization and the latter to an isotropic PAD. While analysis of the FCH_4^- image is straightforward, extraction of the photoelectron eBE spectrum from the *p*-FH_2^- image using the inverse Abel algorithm by Hansen and Law[52] is problematic since the centerline noise falls along the parallel axis and obscures the region with the most signal. The pBasex inversion method[53] is thus advantageous since it produces center point noise. An additional complication arises because photodetachment of FH_2^- not only accesses the reactive $F + H_2$ $^2\Sigma_{1/2}$ state, but also the repulsive, spin–orbit excited $^2\Pi$ states,[15] resulting in lower eKE photoelectrons near the center of the image with a more isotropic PAD. This latter contribution overlaps energetically with the high eBE signal from the transition to the ground electronic state. In an attempt to separate out contributions from the excited states to the photoelectron eBE spectrum, a "parallel" spectrum was constructed in order to capture the

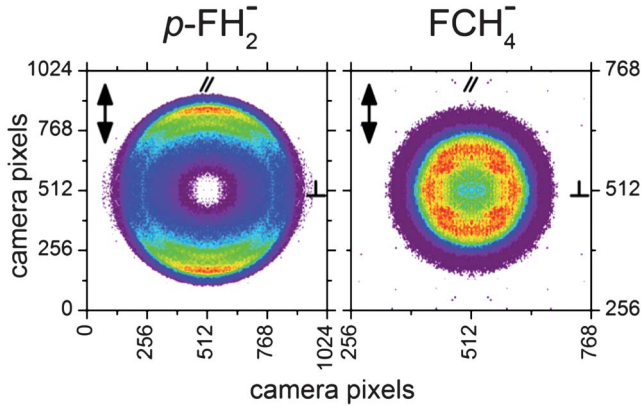

Fig. 2 SEVI images of p-FH_2^- and FCH_4^- showing the p-wave and s-wave nature of the peaks, respectively. The p-FH_2^- image was taken at 311 nm and the FCH_4^- image at 332 nm with laser polarization as indicated by the arrow. Parallel (//) and perpendicular (⊥) regions of the image are labeled.

maximum contribution from a p-wave atomic transition (maxima at 0° and 180° with respect to the laser field) by integrating over two 45° angular slices. A corresponding "perpendicular" spectrum containing contributions from primarily s-wave results was constructed with two 45° slices at 90° and 270° with respect to the laser field. The perpendicular results were subtracted from the parallel results to yield a p-wave only FH_2^- spectrum (See Fig. ESI1 in the Electronic Supplementary Information†). The pBasex image transformation and parallel-perpendicular slice subtraction were done using modified code from Kornilov *et al.*[58]

High-resolution SEVI spectra for n-FH_2^- and p-FH_2^- are shown in Fig. 3 underneath the previous PE results.[11] Fig. 4 shows overview spectra for FCH_4^- and FCD_4^-, while high-resolution spectra of the more intense band around 29900 cm^{-1} are shown in Fig. 5. Peak labels, positions and splittings are listed in Tables 1 and 2.

The overview SEVI spectrum for p-FH_2^- (top black trace in Fig. 3) is dominated by three major bands: a relatively narrow band (**A**) at 29180 cm^{-1}, an intense broad band at 29780 cm^{-1} (**B**) and a weak broad band at 30550 cm^{-1} (**C**). The n-FH_2^- spectrum (Fig. 3) similarly has 3 major bands: a narrow band (**D**) at 29130 cm^{-1} and two intense broad bands at 29490 cm^{-1} (**E**) and 30060 cm^{-1} (**F**). A final very weak band appears around 31000 cm^{-1} (**G**). The overview spectra are similar to previous PE spectra of these anions[11,15] but the peaks are better-resolved, especially for n-FH_2^-. Specifically, band **D** is newly resolved from the neighboring intense band **E**.

As the detachment laser is tuned to the red, and higher resolution, closer-to-threshold images are taken, we observe major relative decreases in peak intensities of the higher eBE features due to the sharp drop-off in photodetachment cross-section for the slowest p-wave electrons owing to the Wigner threshold law, as discussed in Section II. Some fine structure also appears on top of the broad bands: these peaks and shoulders are labeled in lower case and reported in Table 1. We note that the pBasex transformed and subtracted images shown in Fig. 3 show oscillatory noise in low signal-to-noise (S/N) regions like band **G** in the n-FH_2^-results. For this reason, the origin of much of the fine structure is ambiguous, with the notable exception of peaks **a**, **b** and **c** in the p-FH_2^- results, and peak **x** in the n-FH_2^- results, which is essentially a narrower version of band **D**. These weak peaks appear in all the data, including spectra that were transformed using the inverse Abel method and where slices were not subtracted as for the plotted results. Peak **a** appears in the higher resolution scans at 29136 cm^{-1}, nearly lining up with peak **x** at 29121 cm^{-1}. Peaks **c** and **d** appear at 29260 and 29430 cm^{-1} respectively. We

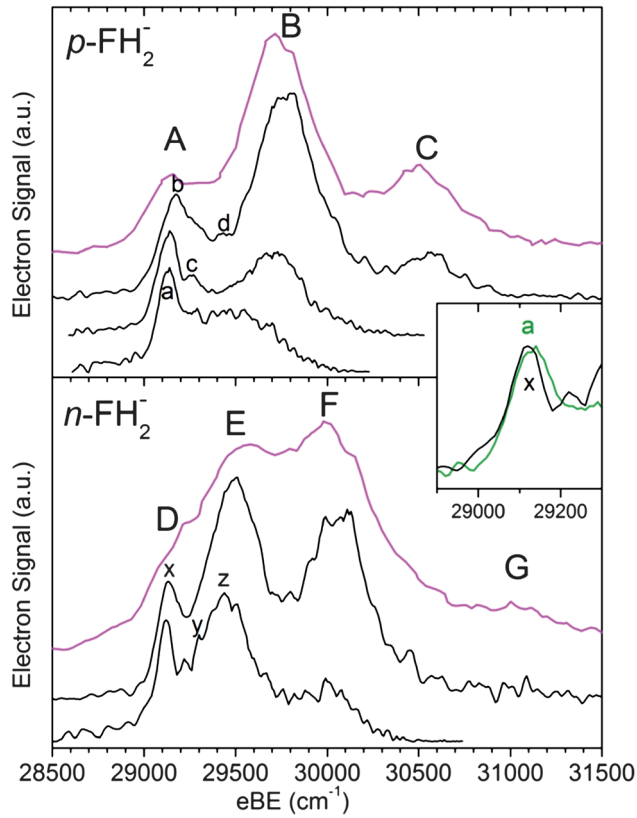

Fig. 3 High resolution SEVI spectra of the *p*-FH_2^- and *n*-FH_2^- anions taken at laser energies of 311 nm (top black trace), 325 nm (next trace) and 329 nm (lower trace, *para* only) showing pBasex transformed and subtracted images (see text). Previous PE results[11] are shown in magenta above the SEVI results. An inset compares the highest resolution scans available for peak **a** (green trace) and peak **x** (black trace).

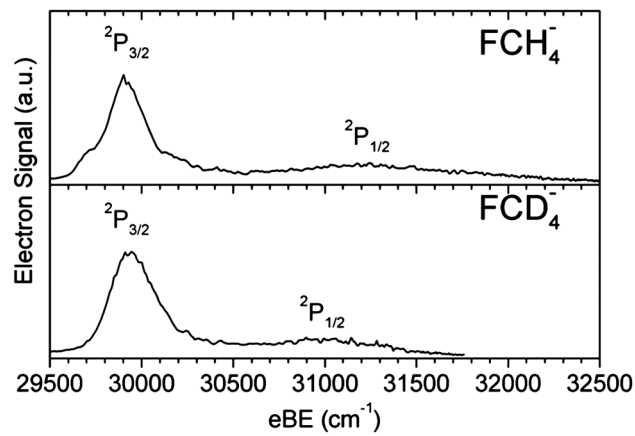

Fig. 4 Overview spectra of the FCH_4^- and FCD_4^- anions taken at 307 nm and 315 nm, respectively, showing transitions to the $^2P_{3/2}$ and $^2P_{1/2}$ spin-orbit states.

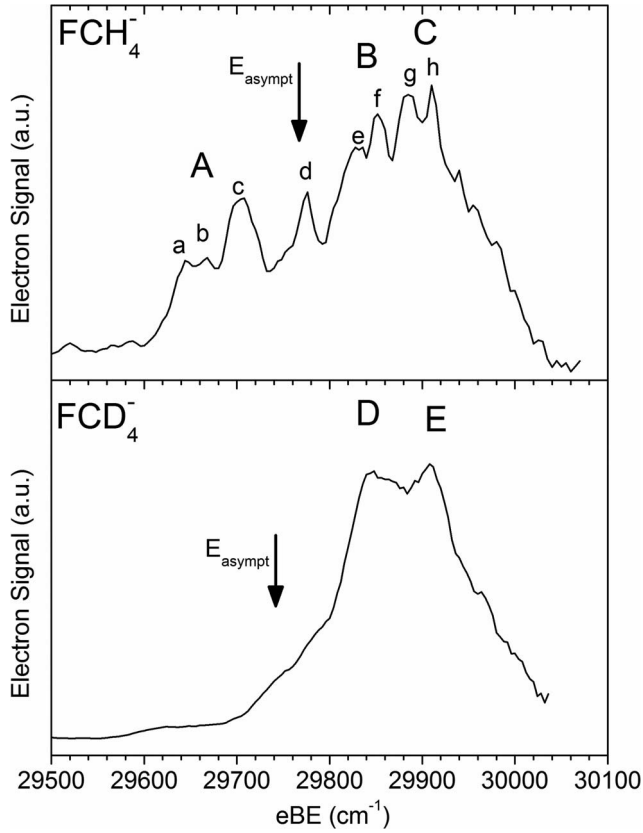

Fig. 5 High resolution SEVI spectra showing transitions to the $^2P_{3/2}$ spin orbit state of FCH_4 and FCD_4. Spectra are spliced together from several high resolution traces taken at 333 nm (see text). Arrow indicates the approximate calculated energy of the reactant asymptote (E_{asympt}).

Table 1 Fine structure of *p*-FH_2^- and *n*-FH_2^- showing position of peaks and the splitting between them

p-FH_2^-				*n*-FH_2^-			
Band	Label	Position (cm^{-1})	Splitting	Band	Label	Position (cm^{-1})	Splitting
A	**a**	29136		**D**	**x**	29121	
	b	29180	44			29225	104
	c	29260	80	**E**	**y**	29300	75
	d	29430	170		**z**	29438	138
B		29768	338	**F**		30044	606
C		30542	774	**G**		30163	281

also note that some fine structure of ambiguous origin labeled **y** and **z** appears in *n*-FH_2^- at close to the same frequencies as peaks **c** and **d**: 29300 cm^{-1} and 29438 cm^{-1}, respectively. Peak **b** appears at 29180 cm^{-1} in the lowest resolution SEVI trace but is never resolved from the neighboring transitions.

SEVI overview spectra for $FCH_4^-$and FCD_4^- are plotted in Fig. 4. Two broad bands are visible for these low resolution spectra, correlating to the $^2P_{3/2}$ (lower eBE) and $^2P_{1/2}$ (higher eBE) spin–orbit states of the fluorine atom. The maximum

of the $^2P_{3/2}$ peak in the FCH_4^- ion appears at 3.709 eV (fwhm = 0.035 eV) while the $^2P_{1/2}$ peak maximum appears 0.160 eV higher at (fwhm = 0.035 eV). The corresponding peaks in the FCD_4^- isotopomer appear at the same position within experimental uncertainty at 3.713 eV (fwhm = 0.032 eV) and 0.128 eV higher at 3.841 eV (fwhm = 0.048 eV). A summary of the peak maxima and spin orbit (SO) splittings appear in Table 2. The splitting of the two bands is similar to that seen previous by Cheng *et al.*,[12] but the $^2P_{3/2}$ band is considerably narrower in our SEVI overview spectrum. The slight shoulder at 29715 cm^{-1} in the FCH_4^- trace in Fig. 4 is the first indication of the rich rovibrational fine structure investigated at higher resolution.

Fig. 5 shows high resolution SEVI spectra of the $^2P_{3/2}$ band of FCH_4^- and FCD_4^-. There are three major bands in the FCH_4^- spectrum: band **A** spanning the 29610–29740 cm^{-1} range, and bands **B** and **C** centered around 29850 cm^{-1} and 29910 cm^{-1} respectively. Bands **A**, **B** and **C** exhibit progressions of closely-spaced peaks, with individual peaks indicated by lower-case letters. The FCD_4^- spectrum comprises two major broad bands **D** and **E** peaking at around 29841 cm^{-1} and 29910 cm^{-1}. For FCH_4^-, the spacing between the two major bands **B** and **C** is ~58 cm^{-1} (peaks **f** and **h**), while it is ~64 cm^{-1} for bands **D** and **E** in the FCD_4^- spectrum. The fine structure comprising **B** and **C** bands averages a 26 cm^{-1} splitting but varies between 20 and 33 cm^{-1}. Upon deuteration, any fine structure overlaying bands **D** and **E** bands is no longer distinguishable at our resolution. This observation suggests that these features are due to motions involving the substituted deuterium atoms, and not due to low S/N artifacts. The fine features in the FCH_4^- spectrum have a fwhm ≈ 30 cm^{-1} (based on a convolution of all the peaks in FCH_4^- bands **A**, **B** and **C**.

The SEVI spectrum for FCH_4^- is spliced together from 4 averaged spectra at −200 V or −350 V VMI, all taken at wavelengths around 332 nm and varying by about 0.2 nm image-to-image to attempt to eliminate systematic noise. Intensities of the spliced spectra were adjusted to match the averaged envelope shape for all spectra taken at −350 V VMI. The appearance of the fine structure present in Fig. 5 varied in intensity and resolution depending on the day and VMI voltage, but never in energy. The FCD_4^- results were similarly constructed from the spliced and intensity scaled portions from 4 averaged spectra. Figs. ESI2 and ESI3 in the Electronic Supplementary Information show the separate traces and the invariance of peak positions.†

IV. Discussion

The FH_2^- and FCH_4^- anions are superficially similar species, though comparison of their SEVI spectra shows quite different characteristics. Relatively little structure is visible for the smaller *p*-FH_2^- and *n*-FH_2^- species while the larger FCH_4^- and

Table 2 Fine structure of the $^2P_{3/2}$ band of FCH_4^- and FCD_4^- showing position of peaks and the splitting between them.[a]

FCH_4^-				FCD_4^-		
Band	Label	Position (cm^{-1})	Splitting	Band	Position (cm^{-1})	Splitting
A	**a**	29644		**D**	29844	
	b	29668	24	**E**	29908	64
	c	29700	32			
	d	29776	76			
B	**e**	29832	56			
	f	29852	20			
C	**g**	29885	33			
	h	29910	25			

[a] Peak positions are ±2 cm^{-1}.

FCD_4^- ions show broad structure with regular progressions of closely-spaced peaks for FCH_4^-. The explanation for this effect lies in the second major difference between the SEVI results: the overall anisotropy of the images differs greatly between systems, with FH_2^- yielding *p*-wave images and FCH_4^- yielding isotropic *s*-wave images (see Fig. 2).

The ejected electron anisotropies are characteristic of the electronic state of the resulting neutral: $^2\Sigma_{1/2}$ for F + H_2 and $^2A_1$ for F + CH_4.[15,28] Owing to the Wigner threshold law[57] (Section II), we can obtain good signal-to-noise on features in the FCH_4^- much closer to threshold, where the resolution is best. Thus, for example, the fwhm of peak **d** in the FCH_4^- spectrum is 17 cm^{-1} (2 meV) when measured at 162 cm^{-1} from threshold. On the other hand, the narrowest peak measured in the FH_2^- system was peak **x** (fwhm = 90 cm^{-1} = 11 meV) which was taken much farther from threshold at 1647 cm^{-1}.

1. *p*-FH_2^- and *n*-FH_2^-

Fig. 6 compares SEVI spectra taken at 325 nm for *p*-FH_2^- and *n*-FH_2^- with the simulated spectra of Russell and Manolopoulos[16] (RM, left panels) and Hartke and Werner[17] (HW, right panels). The simulated spectra assumed an energy resolution of 1 meV, which, as discussed above, is better than that of the SEVI spectra for these anions. In making Fig. 6, anion dissociation energies D_0 of 0.205 and 0.1938 eV were used for RM and HW, respectively, as per the original publications.[11,17] In the following discussion, simulated quantum states are labeled according to their origin from the product (primed) or reactant side (unprimed), and numbered according to the quanta of excitation in the H–H (v) or H–F stretch (v'), the hindered H_2 (j) or HF (j') rotation, and the vdW stretch coordinate F–H_2 (t) or H–HF (t').

We first compare the positions of the broader experimental bands **A–F** to the simulations. The relevant selection rules for photodetachment from *p*-FH_2^- and *n*-FH_2^- have been discussed in detail previously.[15] According to RM, the dominant contributions to peaks **A**, **B**, and **C** in the *p*-FH_2^- photoelectron spectrum are from transitions to the direct scattering states ($v = 0$, $j = 0$, 2, 4), where v refers to the H_2 vibrational quantum number and j to the FH_2 hindered rotor state (very close to a H_2 free rotation). The first three such transitions are marked by an * in Fig. 6. The remaining features are due to resonance states localized in the reactant or product valleys of the F + H_2 surface, which are generally somewhat narrower

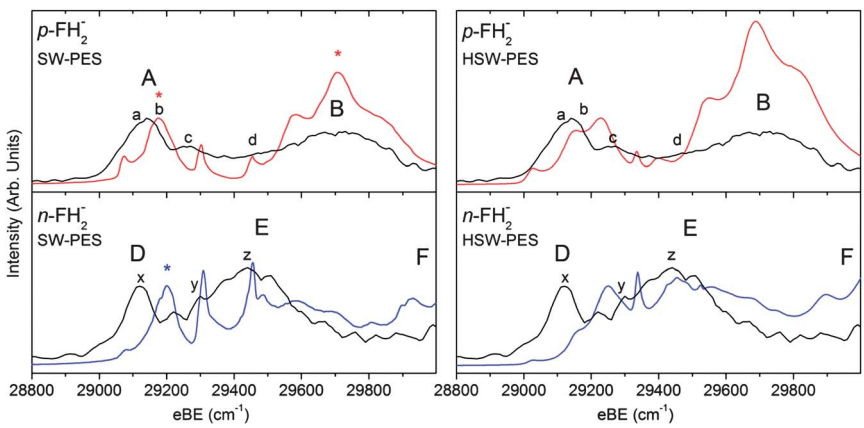

Fig. 6 Comparison of *p*- and *n*-FH_2^- SEVI spectra taken at 325 nm (black traces) with simulated results using the SW-PES[1] and the HSW-PES[2]. Red traces correspond to simulated *p*-FH_2 spectra and blue to *n*-FH_2^- (a 3 : 1 ratio of *ortho* : para). Simulated direct scattering states are indicated with an * (see text).

than the peaks associated with direct scattering states. Upon first glance, the *n*-FH_2^- bands **E**, **F** and **G** would then be assigned to the ($v = 0$, $j = 1$, 3, 5) direct scattering states by their strong intensities and by their positions in relation to the even j peaks for *p*-FH_2^-. In the *n*-FH_2^- simulations however, the direct scattering transition to the ($v = 0, j = 1$) state appears between peaks **D** and **E**, the ($v = 0, j = 3$) state contributes to peak **F**, and several resonance features are also seen. The ($v = 0$, $j = 1$) state lies only 3 meV above the ($v = 0$, $j = 0$) state in the simulations by RM. The main difference in the HW simulations is that the resonance peaks are reduced relative to the direct features, an effect attributed to the slightly larger barrier on the HSW neutral surface used in their simulations (bent barriers for SW and HSW are 535 cm^{-1} and 668 cm^{-1}, respectively[59]). Peaks in the HW simulations are also at slightly higher eBE, in general. HW also note that the near degeneracy of the ($v = 0$, $j = 0$) and ($v = 0$, $j = 1$) states reflects a small tunneling splitting due to the double-minimum well at the TS of the SW-PES. The positions of bands **A**, **B**, **C** and **E**, **F** provide a benchmark for the simulation and testing of the hindered rotor potential at the transition state of FH_2.

We next focus on comparing the finer structure seen in the SEVI data to the simulations, particularly the spectral region around **A** and **D**. This is complicated by the noise level in the experimental spectra, but the features labeled with lower-case letters offer some interesting points of comparison. For example, peak **c**, in the *p*-FH_2^- spectrum and the shoulder **y** in *n*-FH_2^- line up with a feature in the RM simulations assigned to the ($v' = 3$, $j' = 0$, $t' = 0$) product resonance state. In the simulated *p*–FH_2^- spectrum, this product resonance is also the most intense, and happens to be well-separated from the neighboring direct scattering peaks, making it the best candidate for experimental detection. This is the same resonance that has been definitively identified in crossed beam experiments on F + HD.[23,36-39] The neighboring ($v' = 3$, $j' = 2$, $t' = 0$) product reactive resonance then lines up with **d** in the top SEVI *p*-FH_2^- trace and **z** in the bottom *n*-FH_2^- trace of Fig. 3.

However, the most interesting comparison involves peaks **a**, **b**, and **x**. Although peaks **a** and **b** do not appear as two distinct features at any photon energy, Fig. 3 shows that as the photon energy is lowered, the band **A** maximum shifts to lower eBE and becomes narrower. If peak **b** were simply due to an unresolved contribution of peak **a** and **c**, we would expect either a shifted broad maximum, or a non-shifted narrower peak with a shoulder. Since we observe both a shift and a shoulder, it seems that band **A** might comprise *three* unresolved transitions, **a**, **b** and **c**, with an increase in relative intensity of peak **a** close to threshold. Such an effect could be due to differences in anisotropy with peak **a** (and possibly **c**) having more *s*-wave character and peak **b** having more *p*-wave character, causing peak **a** to persist even close to threshold. Unfortunately, the peaks comprising band **A** are not fully resolved and so we are unable to distinguish between the anisotropies (in the form of beta parameters[51]) of these peaks. Differences in intrinsic peak width could also cause the observed intensity behavior of peaks **a**, **b** and **c**, with narrow transitions retaining significant intensity close to threshold while the higher eBE portion of a broader peak disappears. Differences in peak widths are indeed expected for this system, with direct-scattering states being broader than resonance states.[16]

Comparing the *n*-FH_2^- and *p*-FH_2^- SEVI spectra, we find that at the lowest photodetachment energy, the Gaussian-fit center of peak **a** occurs 15 cm^{-1} *higher* than peak **x**. However, peak **a** is significantly broader than peak **x** (118 cm^{-1} *versus* 90 cm^{-1}), and the rising edges of both **x** and **a** match up exactly, as shown in the inset in Fig. 3. This comparison suggests that peak **a** is not yet fully resolved from the neighboring peak **b**. There is little evidence for the analog of peak **b** in the *n*-FH_2^- spectrum.

Peaks **a** and **x** each fall between two features in the simulated spectra. Peak **a** lies between the ($v = 0, j = 0, t = 0$) reactant resonant state at 29050 cm^{-1} and the ($v = 0$, $j = 0$) direct scattering peak. Peak **x** lies between the same resonance peak (which is much lower in intensity as it originates from *p*-FH_2^-) and the direct scattering peak dominated by the ($v = 0$, $j = 1$) state. These comparisons suggest two possible

assignments for peaks **a**, **b**, and **x**. First, peak **b** could be the ($v = 0, j = 0$) direct scattering state, with the ($v = 0, j = 1$) state lying considerably higher in energy, perhaps at the band **E** maximum. A larger splitting between these states would be expected for nearly free rotation of the H_2 moiety in the FH_2 complex. Under these circumstances, peaks **a** and **x** would be assigned to resonance states, with their approximately equal binding energies and strong intensities in both p-FH_2^- and n-FH_2^- spectra suggesting they might be product as opposed to reactant resonances. This assignment agrees with earlier analyses of lower resolution PE results.[11]

An alternate assignment arises if peak **b** is not a true peak, but instead simply the maximum of the convolution of peaks **a** and **c**. This would then require that peak **a** be the ($v = 0$, $j = 0$) state, which would appear with some intensity in the n-FH_2^- spectrum as peak **x**. The ($v = 0$, $j = 1$) direct scattering state in the n-FH_2^- spectrum would then be significantly higher in energy, at peak **E**. This assignment is appealing as it does not require the presence of any other reactant or product resonances than **c**, for which there is experimental evidence, and attributes all the most intense features to direct scattering states. However, if peak **x** (band **D**) originates only from the presence of p-FH_2^- in the n-FH_2^-spectrum, we would also expect stronger contributions from the other p-FH_2^- bands, especially in the 311 nm n-FH_2^- SEVI trace where the 311 nm p-FH_2^- results show intense **B** and **C** bands. These contributions are clearly missing, most notably in the 29800 cm^{-1} region of the 311 nm n-FH_2^- SEVI trace (Fig. 3).

Overall, the comparison between the SEVI data and simulated spectra indicates that there are discrepancies between experiment and theory in the low eBE spectra where our signal-to-noise is best. It would be of considerable interest to test the proposed assignments of the peaks in this region by performing simulations based on the more recent potential energy surfaces available for the F + H_2 reaction.[19–23]

2. FCH_4^- and FCD_4^-

In this section, we consider the highly structured FCH_4^- and FCD_4^- SEVI spectra and attempt to interpret them in light of past experimental and theoretical work. Infrared spectroscopy and electronic structure calculations[29,31] indicate that FCH_4^- has C_{3v} symmetry with a linear F–H–C bond arrangement. The most recent calculations[29] find $r_{CF} = 2.955$ Å and $D_0(FCH_4^-) = 0.290$ eV. On the recent F + CH_4 surface reported by Czakó *et al.*,[28] there are two vdW structures in the entrance valley lying 40 and 160 cm^{-1} below the reactant asymptote, and a saddle point 240 cm^{-1} above the reactants. The more weakly bound vdW structure, which is actually a saddle point, has the same C_{3v} structure as the anion but with a considerably longer r_{CF} of 3.6 Å. The other structure, representing a true minimum, also has C_{3v} symmetry with the F atom bound directly to the C atom (*i.e.* back-side bonding) with $r_{CF} = 2.940$ Å. At the TS, calculations at the highest level of theory find a nonlinear F–H–C bond with $\angle FHC = 152.3°$ and $r_{CF} = 2.732$ Å, but the potential energy with respect to this angle is very flat; the optimized TS geometry with $\angle FHC = 180°$ is higher in energy by less than 10 cm^{-1}. Based on these results, as pointed out by Cheng *et al.*,[12] photodetachment of FCH_4^- will probe the reactant side of the F + CH_4 reaction. The Franck–Condon region accessible *via* photodetachment should overlap best with the more strongly bound vdW structure and the reactant side of the transition state region, as indicated in Fig. 1.

We can distinguish the contributions from these two regions to the spectrum by comparing the eBE of each feature to the reactant asymptote E_{asympt}, illustrated in Fig. 1 and defined by

$$E_{asympt} = D_0(FCH_4^-) + EA(F).$$

We find $E_{asympt} = 3.691$ eV (~29770 cm^{-1}) based on the electron affinity of fluorine[60] (EA(F) = 3.401 eV) and $D_0(FCH_4^-)$ given above. Below this energy,

only those states residing within the entrance channel vdW well are expected. In the FCH_4^- spectrum, all features associated with band **A** fall below this asymptote and are thus assigned to bound reactant vdW states. Bands **B** and **C** fall above E_{asympt}, and are attributed to states with energies partway between the reaction asymptote and the TS.[12] The sharp peak **d** matches E_{asympt} almost exactly. In the FCD_4^- spectrum, E_{asympt} is expected to be slightly lower (by $\sim$22 cm^{-1}, difference based on optimized MP2/aug-cc-pVDZ structures) due to the isotope effect on D_0, and only the unresolved low eBE tail extending to $\sim$29600 cm^{-1} falls below it.

The vdW band **A** shows some fine structure labeled **a–d** in Fig. 5, although the inclusion of peak **d** with this band rather than band **B** is somewhat arbitrary. As indicated above, r_{CF} for the anion and more strongly bound reactant vdW structure are quite close, but the orientation of the CH_4 relative to the F atom changes from a linear F–H–C bond conformation in the anion ($\angle FCH = 0°$) to a back-side bonded F–C–H bond conformation in the neutral ($\angle FCH = 70.5°$).[29,28] Under these circumstances, it is reasonable to assign peaks **a–c**, and possibly **d**, to intermolecular bending vibrations or hindered rotation of the CH_4 moiety of this vdW complex; the latter would be consistent with the varying peak spacing with eBE. The lowest eBE feature, peak **a**, lies only 124 cm^{-1} below E_{asympt}, consistent with the calculated binding energy of the lowest energy vdW structure (160 cm^{-1}) relative to F + CH_4.

Intensity in the vdW region of the FCD_4^- spectrum (low eBE tail) is less pronounced. Since the methyl orientations in the anion and lowest energy neutral vdW structure are so different, the Franck–Condon intensity will be governed by an imperfect overlap of the wavefunctions, aided by the shallow neutral potential in the $\angle FCH$ coordinate and the spread-out wavefunctions residing within. We expect the lowest energy vdW state to be less intense in the deuterated species than in the hydrogenated species due to a small decrease in zero-point energy (ZPE) causing a large decrease in wavefunction spread in the shallow neutral potential. Fig. 7 presents a highly schematic version of potential energy *versus* $\angle FCH$ in the anion and neutral. We also expect the best overlap with the anion levels to occur at a higher quantum number state in the deuterated species than in the hydrogenated species due to the smaller level spacing. In any case, it is unlikely that the usual Franck–Condon/harmonic oscillator picture for analyzing photoelectron spectra will be sufficient to interpret the vdW features in the SEVI of spectra of the two isotopologs; a full multidimensional quantum treatment along the lines of that used to simulate the ClH_2^- SEVI spectrum will probably be needed.[33]

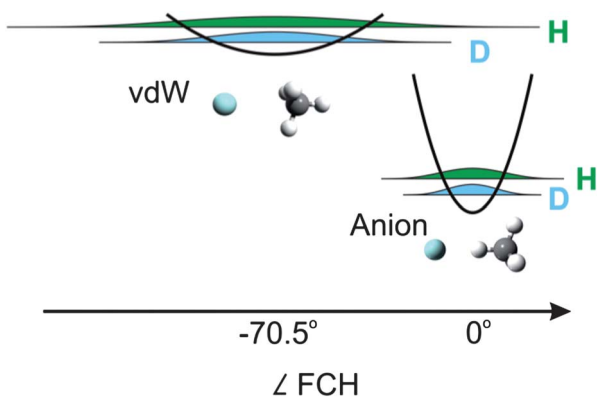

Fig. 7 Schematic potential energy diagram as a function of F–C–H angle ($\angle FCH$) showing comparative wavefunction spread for hydrogenated and deuterated species in the shallow vdW well and in the deep anion well.

The remaining region of the spectrum (bands **B** and **C**; **D** and **E**) shows progressions with an average spacing of 26 cm^{-1} in FCH_4^-. These regions exhibit two intensity maxima separated by 58 and 64 cm^{-1} for the two isotopologs. All of this structure lies above the reactant asymptote (E_{asympt}), peaking at a vertical detachment energy (VDE) of E_{asympt} + 126 cm^{-1} (see Fig. 5) and extending to about 300 cm^{-1} above E_{asympt} (see Fig. 4). These values are near to the previous VDE[12] estimate of E_{asympt} + 100 cm^{-1} and the calculated TS energy[28] of 240 cm^{-1} above E_{asympt}, respectively, indicating that any structure underlying **B**, **C**, **D** and **E** corresponds either to direct scattering states or resonances near the transition state but primarily on the reactant side. Taking the calculated saddle point geometry as a reference point, there are significant changes upon photodetachment in $\angle$FCH and r_{CF}, as mentioned above, which would lead to low frequency progressions in intermolecular bending modes and the intermolecular F···CH_4 stretch. To first order, these modes are perpendicular and parallel, respectively, to the reaction coordinate in the entrance valley. Under this assumption, direct scattering states would be quantized with respect to the intermolecular bend or hindered CH_4 rotation (along with all the other higher frequency vibrational modes), whereas resonances states, as in F + H_2, would be additionally quantized along the intermolecular stretch frequency.

The fine structure comprising bands **B** and **C** can be compared to the available calculated frequencies for the TS of the neutral. The TS of FCH_4 has an imaginary intermolecular stretching frequency at 357*i*(246*i*) cm^{-1}, and two intermolecular bending vibrations at 40(277) cm^{-1} and at 117(344) cm^{-1} with a' and a'' symmetry, respectively.[28] These values are all harmonic, calculated from the PES fundamental (or from *ab initio* structures). None of the calculated TS frequencies are in particularly good agreement with peak spacings in the SEVI spectra. However, treating the intermolecular bend as a harmonic vibration is unlikely to be very accurate, as the bend potential at the transition state is very anharmonic and flat, with shallow minima separated by small barriers. Hence, one might expect a considerably lower frequency for the intermolecular bend than the harmonic value, or, alternatively, hindered rotor structure with peaks spaced much more closely than the harmonic bend frequency. Both bending and hindered rotor levels would display a substantial isotope effect in going from CH_4 to CD_4 that would be much less pronounced for an intermolecular stretching mode. These considerations suggest assigning the 26 cm^{-1} progression to large amplitude intermolecular bend vibrations or hindered rotations.

The question then arises as to whether the fine structure in the spectrum represents direct scattering states or resonance structure. It is difficult to resolve this issue in the absence of high level calculations. However, the experimental peaks are narrower (fwhm $\approx$ 27 cm^{-1}) than the direct scattering features in the FH_2^- simulations (fwhm $\approx$ 76 cm^{-1}), suggesting that they arise from resonance states. If this is the case, then the $\sim$58 cm^{-1} spacing underlying the fine structure might represent a progression along the reaction coordinate, primarily involving the intermolecular F···CH_4 stretch. The calculated frequency[29] of the corresponding mode in the anion is 200 cm^{-1}, and a substantially lower value for the corresponding quasi-bound mode in the neutral is reasonable. Moreover, this mode should exhibit a minimal isotope effect as it primarily involves heavy atom motion, consistent with the observation of similar spacings in the SEVI spectra of FCH_4^- and FCD_4^-.

The interpretation of the results shown here is necessarily simplistic. For example, the assignment of a single internal coordinate as the reaction coordinate is a questionable approximation, given that r_{CH}, r_{HF}, and $\angle$FCH, where H refers to the hydrogen atom being transferred, all evolve along the minimum energy path in the reactant valley.[28] What is unambiguous from our experiment is the observation of narrower features than have ever been seen in any of our transition state spectroscopy experiments with the exception of IHI^-, where we clearly were observing resonances.[34]

The SEVI spectroscopy of the $FCH_4 \leftarrow FCH_4^-$ system can improve the understanding of the bimolecular reaction by providing experimental features with which to test the currently available F + CH_4 and FCH_4^- PES.[28-30] Crossed beam experiments on the F + CH_4 reaction have shown results such as product selectivity due to reactant vibrational excitation that depend on the exact location of the TS. The identification of resonances on the reactant side of the TS (*versus* the previously identified reactive resonances in the HF($v' = 3$) product region)[5,41] could have implications on the dynamics of the bimolecular reaction. Additionally, the properties of the reactant vdW region are especially important in low collision energy cross beam experiments, as suggested by the increased FD product selectivity in the F + $CHD_3(\nu_1 = 1)$ reaction at low collision energies.[61] The vdW region has proven particularly difficult to simulate,[28] and so the observed vdW structure, which shows multiple peaks and a strong isotope dependence, may well provide the experimental motivation for a detailed exploration of this surface including accurate frequencies and barriers to interconversion of the two different vdW structures.

V. Conclusions

Here we present a set of high resolution negative ion photoelectron spectra for *p*-FH_2^-, *n*-FH_2^-, FCH_4^- and FCD_4^- ions, improving on previously published results and showing transitions to states at or near the TS of the F + H_2 or F + CH_4 bimolecular reactions. The higher resolution spectra for *p*-FH_2^- resolve a new peak **a** observable only close to threshold, while the spectra for *n*-FH_2^- completely resolve a previously observed shoulder **x**. These two lowest energy peaks are significantly narrower than the other features and occur at the same position in both spectra, disagreeing with previous assignments. A narrow peak is identified and tentatively assigned to the ($v' = 3, j' = 0, t' = 0$) product resonance state, the same resonance that has been seen in crossed beam experiments on F + HD.[23,36-39] The experimental results suggest that improvements are needed in the SW-PES and HSW-PES, in particular for the bending potential in the TS region. High resolution spectra of the FCH_4^- $^2P_{3/2}$ states reveal a rich fine structure, with peak progressions spaced by 26 cm^{-1}. We attribute this structure to the bending or hindered rotation of the methyl moiety with respect to the fluorine atom. A band attributed to bound vdW states is also observed in the FCH_4^- spectrum, and shows significant changes upon deuteration. We attribute this to the isotope effect, which decreases the neutral vdW cluster ZPE and level spacings resulting in differing Franck–Condon overlap of the anion and neutral states.

Much is left to be unraveled in the SEVI spectra of these TS systems. We hope that, given the availability of increasingly accurate PES and the documented procedures for simulation of photoelectron results including quantum effects like reactive resonances,[16,17] theoretical comparisons might soon be available for the FCH_4^- and FCD_4^- spectra. Treatment of the hindered rotation in such a system is also an interesting problem all on its own. Conversely, we also hope that these SEVI results will allow for further testing and validation of both the F + CH_4 and F + H_2 PES by providing a direct probe of the TS region and complementing the numerous available crossed beam studies.

Acknowledgements

This work was supported by the Air Force Office of Scientific Research under grant numbers FA9550-09-1-0343 and F49620-03-1-0085. We thank Oleg Kornilov for use of his program to perform the pBasex transform and wedge subtractions. We also thank David Manolopoulos and Gabor Czakó for helpful discussions. T.I.Y. and E.G. thank the National Science and Engineering Research Council of Canada (NSERC) for post graduate scholarships. C.H. is supported by a postdoctoral scholarship from the German Academic Exchange Service (DAAD).

Notes and references

1 D. M. Neumark, A. M. Wodtke, G. N. Robinson, C. C. Hayden and Y. T. Lee, *J. Chem. Phys.*, 1985, **82**, 3045–3066.
2 D. E. Manolopoulos, *J. Chem. Soc., Faraday Trans.*, 1997, **93**, 673–683.
3 K. P. Liu, *Annu. Rev. Phys. Chem.*, 2001, **52**, 139–164.
4 W. F. Hu and G. C. Schatz, *J. Chem. Phys.*, 2006, **125**, 132301.
5 W. Shiu, J. J. Lin and K. P. Liu, *Phys. Rev. Lett.*, 2004, **92**, 103201.
6 W. Q. Zhang, H. Kawamata and K. P. Liu, *Science*, 2009, **325**, 303–306.
7 J. Zhou, J. J. Lin and K. Liu, *Mol. Phys.*, 2010, **108**, 957–968.
8 N. Balucani, G. Capozza, F. Leonori, E. Segoloni and P. Casavecchia, *Int. Rev. Phys. Chem.*, 2006, **25**, 109–163.
9 K. P. Liu, *J. Chem. Phys.*, 2006, **125**, 132307.
10 D. M. Neumark, *Phys. Chem. Chem. Phys.*, 2005, **7**, 433–442.
11 D. E. Manolopoulos, K. Stark, H. J. Werner, D. W. Arnold, S. E. Bradforth and D. M. Neumark, *Science*, 1993, **262**, 1852–1855.
12 M. Cheng, Y. Feng, Y. K. Du, Q. H. Zhu, W. J. Zheng, G. Czakó and J. M. Bowman, *J. Chem. Phys.*, 2011, **134**, 191102.
13 S. E. Bradforth, D. W. Arnold, R. B. Metz, A. Weaver and D. M. Neumark, *J. Phys. Chem.*, 1991, **95**, 8066–8078.
14 A. Weaver and D. M. Neumark, *Faraday Discuss. Chem. Soc.*, 1991, **91**, 5–16.
15 S. E. Bradforth, D. W. Arnold, D. M. Neumark and D. E. Manolopoulos, *J. Chem. Phys.*, 1993, **99**, 6345–6359.
16 C. L. Russell and D. E. Manolopoulos, *Chem. Phys. Lett.*, 1996, **256**, 465–473.
17 B. Hartke and H. J. Werner, *Chem. Phys. Lett.*, 1997, **280**, 430–438.
18 K. Stark and H. J. Werner, *J. Chem. Phys.*, 1996, **104**, 6515–6530.
19 M. Hayes, M. Gustafsson, A. M. Mebel and R. T. Skodje, *Chem. Phys.*, 2005, **308**, 259–266.
20 M. H. Qiu, Z. F. Ren, L. Che, D. X. Dai, S. A. Harich, X. Y. Wang, X. M. Yang, C. X. Xu, D. Q. Xie, M. Gustafsson, R. T. Skodje, Z. G. Sun and D. H. Zhang, *Science*, 2006, **311**, 1440–1443.
21 C. X. Xu, D. Q. Xie and D. H. Zhang, *Chin. J. Chem. Phys.*, 2006, **19**, 96–98.
22 G. L. Li, H. J. Werner, F. Lique and M. H. Alexander, *J. Chem. Phys.*, 2007, **127**, 174302.
23 Z. Ren, L. Che, M. Qiu, X. Wang, W. Dong, D. Dai, X. Wang, X. Yang, Z. Sun, B. Fu, S.-Y. Lee, X. Xu and D. H. Zhang, *Proc. Natl. Acad. Sci. U. S. A.*, 2008, **105**, 12662–12666.
24 J. F. Castillo, F. J. Aoiz, L. Banares, E. Martinez-Nunez, A. Fernandez-Ramos and S. Vazquez, *J. Phys. Chem. A*, 2005, **109**, 8459–8470.
25 D. Troya, *J. Chem. Phys.*, 2005, **123**, 214305.
26 T. S. Chu, X. Zhang, L. P. Ju, L. Yao, K. L. Han, M. L. Wang and J. Z. H. Zhang, *Chem. Phys. Lett.*, 2006, **424**, 243–246.
27 J. Espinosa-Garcia, J. L. Bravo and C. Rangel, *J. Phys. Chem. A*, 2007, **111**, 2761–2771.
28 G. Czakó, B. C. Shepler, B. J. Braams and J. M. Bowman, *J. Chem. Phys.*, 2009, **130**, 084301.
29 G. Czakó, B. J. Braams and J. M. Bowman, *J. Phys. Chem. A*, 2008, **112**, 7466–7472.
30 G. Czakó and J. M. Bowman, *Phys. Chem. Chem. Phys.*, 2011, **13**, 8306–8312.
31 Z. M. Loh, R. L. Wilson, D. A. Wild, E. J. Bieske and M. S. Gordon, *Aust. J. Chem.*, 2004, **57**, 1157–1160.
32 D. M. Neumark, *Acc. Chem. Res.*, 1993, **26**, 33–39.
33 E. Garand, J. Zhou, D. E. Manolopoulos, M. H. Alexander and D. M. Neumark, *Science*, 2008, **319**, 72–75.
34 I. M. Waller, T. N. Kitsopoulos and D. M. Neumark, *J. Phys. Chem.*, 1990, **94**, 2240–2242.
35 J. C. Polanyi and A. H. Zewail, *Acc. Chem. Res.*, 1995, **28**, 119–132.
36 R. T. Skodje, D. Skouteris, D. E. Manolopoulos, S. H. Lee, F. Dong and K. Liu, *J. Chem. Phys.*, 2000, **112**, 4536–4552.
37 F. Dong, S. H. Lee and K. Liu, *J. Chem. Phys.*, 2000, **113**, 3633–3640.
38 R. T. Skodje, D. Skouteris, D. E. Manolopoulos, S. H. Lee, F. Dong and K. P. Liu, *Phys. Rev. Lett.*, 2000, **85**, 1206–1209.
39 W. Dong, C. Xiao, T. Wang, D. Dai, X. Yang and D. H. Zhang, *Science*, 2010, **327**, 1501–1502.
40 J. G. Zhou, J. J. Lin and K. P. Liu, *J. Chem. Phys.*, 2004, **121**, 813–818.
41 G. Czakó, Q. A. Shuai, K. P. Liu and J. M. Bowman, *J. Chem. Phys.*, 2010, **133**, 131101.
42 A. Osterwalder, M. J. Nee, J. Zhou and D. M. Neumark, *J. Chem. Phys.*, 2004, **121**, 6317–6322.
43 D. M. Neumark, *J. Phys. Chem. A*, 2008, **112**, 13287–13301.
44 A. Eppink and D. H. Parker, *Rev. Sci. Instrum.*, 1997, **68**, 3477–3484.

45 U. Even, J. Jortner, D. Noy, N. Lavie and C. Cossart-Magos, *J. Chem. Phys.*, 2000, **112**, 8068–8071.
46 E. Garand, T. I. Yacovitch and D. M. Neumark, *J. Chem. Phys.*, 2009, **130**, 064304–064307.
47 J. Zhou, E. Garand, W. Eisfeld and D. M. Neumark, *J. Chem. Phys.*, 2007, **127**, 034304.
48 T. Theis, P. Ganssle, G. Kervern, S. Knappe, J. Kitching, M. P. Ledbetter, D. Budker and A. Pines, *Nat. Phys.*, 2011, **7**, 571–575.
49 W. C. Wiley and I. H. McLaren, *Rev. Sci. Instrum.*, 1955, **26**, 1150–1157.
50 D. W. Chandler and P. L. Houston, *J. Chem. Phys.*, 1987, **87**, 1445–1447.
51 A. Sanov and R. Mabbs, *Int. Rev. Phys. Chem.*, 2008, **27**, 53–85.
52 E. W. Hansen and P.-L. Law, *J. Opt. Soc. Am. A*, 1985, **2**, 510–519.
53 G. A. Garcia, L. Nahon and I. Powis, *Rev. Sci. Instrum.*, 2004, **75**, 4989–4996.
54 V. Dribinski, A. Ossadtchi, V. A. Mandelshtam and H. Reisler, *Rev. Sci. Instrum.*, 2002, **73**, 2634–2642.
55 U. Berzinsh, M. Gustafsson, D. Hanstorp, A. Klinkmuller, U. Ljungblad and A. M. Martenssonpendrill, *Phys. Rev. A: At., Mol., Opt. Phys.*, 1995, **51**, 231–238.
56 C. Blondel, *Phys. Scr.*, 1995, **T58**, 31–42.
57 E. P. Wigner, *Phys. Rev.*, 1948, **73**, 1002–1009.
58 O. Kornilov, C. C. Wang, O. Bunermann, A. T. Healy, M. Leonard, C. Peng, S. R. Leone, D. M. Neumark and O. Gessner, *J. Phys. Chem. A*, 2010, **114**, 1437–1445.
59 J. F. Castillo, B. Hartke, H. J. Werner, F. J. Aoiz, L. Banares and B. Martinez-Haya, *J. Chem. Phys.*, 1998, **109**, 7224–7237.
60 C. Blondel, C. Delsart and F. Goldfarb, *J. Phys. B: At., Mol. Opt. Phys.*, 2001, **34**, L281–L288.
61 G. Czakó and J. M. Bowman, *J. Am. Chem. Soc.*, 2009, **131**, 17534–17535.

